Estuarine, Coastal and Shelf Science 111 (2012) 60–66

Contents lists available at SciVerse ScienceDirect

Estuarine, Coastal and Shelf Science

journal homepage: www.elsevier.com/locate/ecss

# About the tidal oscillations of temperature in a tidally driven estuary: The case of Guadalquivir estuary, southwest Spain

Jesús García-Lafuente [a,*], Javier Delgado [a], Gabriel Navarro [b], Concepción Calero [a], Manuel Díez-Minguito [c], Javier Ruiz [b], José C. Sánchez-Garrido [a]

[a] Physical Oceanography Group, CEIMAR, University of Málaga, Málaga, Spain
[b] Department of Ecology, Instituto de Ciencias Marinas de Andalucia ICMAN-CSIC, Puerto Real, Spain
[c] Grupo de Dinámica de Flujos Ambientales, University of Granada, Granada, Spain

ARTICLE INFO

*Article history:*
Received 20 January 2012
Accepted 18 June 2012
Available online 14 July 2012

*Keywords:*
estuary
temperature oscillations
Guadalquivir river
Gulf of Cadiz
radiational tide
harmonic analysis

ABSTRACT

An 18-month time series of temperature collected in the vicinity of the Guadalquivir estuary mouth has been analyzed to investigate tidal signals in the temperature records. Two sources of similar importance are acting jointly to produce these signals, the gravitational tide generating potential that acts through the tidal currents induced by the vertical tide at the estuary's mouth and the radiational potential whose origin is the sun's radiation. The most important signal is the radiational diurnal S1, which exhibits a seasonal modulation. The next one in importance is M2, introduced via the advective term, which shows semiannual modulation due to the change of sign of the horizontal temperature gradient. The S2 constituent is a mixture of radiational (via the first harmonic of S1) and gravitational contributions, the former being about twice the latter. The harmonic constants of all these constituents are time-dependent so that caution is needed to interpret results deduced from time series of few months.


## 1. Introduction

The Guadalquivir river flows into the Gulf of Cadiz, North Atlantic Ocean, through a very long (O (100 km)) estuary whose freshwater discharge is controlled by a manmade dam at Alcala del Rio (Fig. 2). The river discharge is partially seasonal with very limited flow in summertime and sporadic floods in late winter–early spring (the wet season) that follow intensive rainfall episodes (Navarro et al., 2011). The main driving mechanism is the tidal forcing at the mouth whose M2 amplitude is around 1 m in the nearby city of Cadiz (García-Lafuente et al., 1990). Taking into account the contribution of other relevant semidiurnal and diurnal tidal constituents the tidal range would be around 3 m (Rodríguez-Ramirez and Yáñez-Camacho, 2008) that, according to Davies (1964) classification, situates the Guadalquivir estuary into the meso-tidal category. Tidal wave is predominantly progressive with some features of standing wave and penetrates around 100 km inland (Alvarez et al., 2001). The low mean river discharge along with the high tidal prism associated to the large tidal range and the small depth of the channel (about 8 m in the mid-channel on average) make the Guadalquivir estuary be a well-mixed estuary with very small vertical salinity/temperature gradients.

The sea surface temperature of Gulf of Cadiz, which is located at mid-latitude in the northern hemisphere, undergoes a noticeable seasonal cycle (García-Lafuente et al., 2004; see also Fig. 3) which is locally enhanced off Guadalquivir river mouth by coastal processes. This feature, already reported in Vargas et al. (2003) and García-Lafuente and Ruiz (2007), is thought to play a significant role in the Gulf of Cadiz inner-shelf circulation and in the life cycle of fish species of commercial interest (Ruiz et al., 2006).

The joint effect of the temperature gradient generated at the estuary mouth and within the estuary itself, the relatively important tidal forcing and the heating of water by the solar radiation (see sketch in Fig. 1 and caption there) gives place to different periodic signals of tidal frequencies in the local temperature records that deserve a detailed analysis. A common technique to investigate these tidal signals is the harmonic analysis that is usually carried out through standard software packages, among which the so called T_Tide (Pawlowicz et al., 2002) is probably the most widely used. The routinary use of this software can lead, however, to erroneous conclusions when dealing with water temperature series in estuaries. This work analyses such temperature signals. In Section 2 we present the dataset. Sections 3.1 and

* Corresponding author. ETSI Telecomunicación, Campus de Teatinos, 29071 Málaga, Spain.
*E-mail address:* glafuente@ctima.uma.es (J. García-Lafuente).

0272-7714/$ – see front matter © 2012 Elsevier Ltd. All rights reserved.
http://dx.doi.org/10.1016/j.ecss.2012.06.007

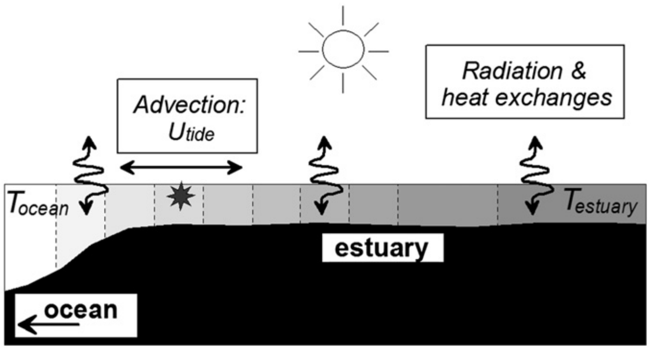


**Fig. 1.** Sketch showing the two main processes inducing periodic signals in local temperature records at a site nearby the estuary mouth (black star). Estuarine waters are represented by the shaded areas that indicate a progressive variation of temperature from the ocean ($T_{ocean}$) to the upper estuary ($T_{estuary}$). As far as the estuary is well-mixed, isotherms are vertical (dashed lines) and temperature only has horizontal gradient. The gradient induces local oscillations of temperature when advected by the tidal currents (represented by the double-headed horizontal arrow). The double-headed winding arrows indicate the air–sea heat exchanges among which the short-wave solar radiation is fundamental. These heat exchanges spread all over the estuary with similar intensity and are not particularly space-dependent.

3.2 investigate their origin, while Sections 3.3 and 3.4 deal with their time dependence and highlights some erroneous results that could be obtained using conventional tidal analysis software. Section 3.5 discusses the validity of our approach by analyzing the horizontal temperature gradient and, finally, Section 4 summarizes our conclusions.

## 2. Data

Surface temperature (1 m below sea surface) and velocity at seven different levels were registered every 15 min by a down-looking Acoustic Doppler Profiler (ADP) placed 9 km upstream of the Guadalquivir estuary's mouth in the central part of the channel (location B7 hereinafter, see Fig. 2) from 01/07/2008 to 24/10/2009. The ADP was a Nortek AS Aquadopp of 1 MHz frequency with nominal accuracy of 1% of the measured velocity. The thermistor measuring temperature, embedded in the ADP, has nominal accuracy and resolution of 0.1 °C and 0.01 °C, respectively. More details on the sensor equipment deployed in B7 can be seen in Navarro et al. (2012).

Sea surface temperature (SST) from infrared imagery was used to illustrate the seasonal cycle of SST at two sites in the Gulf of Cadiz, namely an open sea site and a second site nearby the estuary mouth (GC and GU, respectively, in Fig. 2). Finally, long in situ observations of surface temperature close to the river bank at two sites well upstream the estuary (MR and GL, Fig. 2) were downloaded from the "Red Automática de Vigilancia y Control de la Calidad del Agua" of the Junta de Andalucía website. Fig. 3A shows several years of the temperature series available in this study and Fig. 3B shows a zoom of Fig. 3A in which the tidal-frequency oscillations are easily distinguishable.

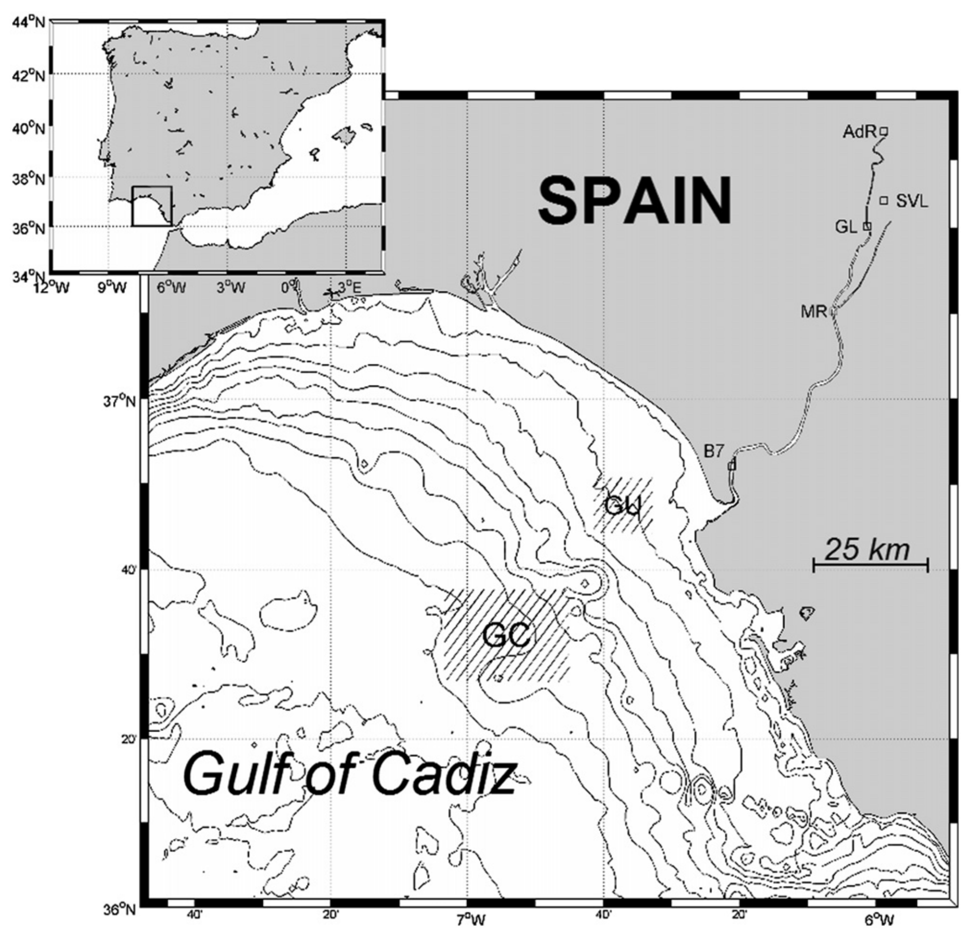


**Fig. 2.** Map showing the geographical position of the Guadalquivir estuary, in the Gulf of Cadiz area. Acronyms indicate the position of the locations mentioned in the text: GC and GU are the areas where SST has been spatially averaged to provide GC and GU temperature series, respectively; B7 is the position of the buoy where the bulk of data in this study comes from; MR and GL indicate the upstream locations of El Marmol and Gelves temperature stations; AdR is the site where Guadalquivir river is dammed and SVL indicates the location of Seville city.

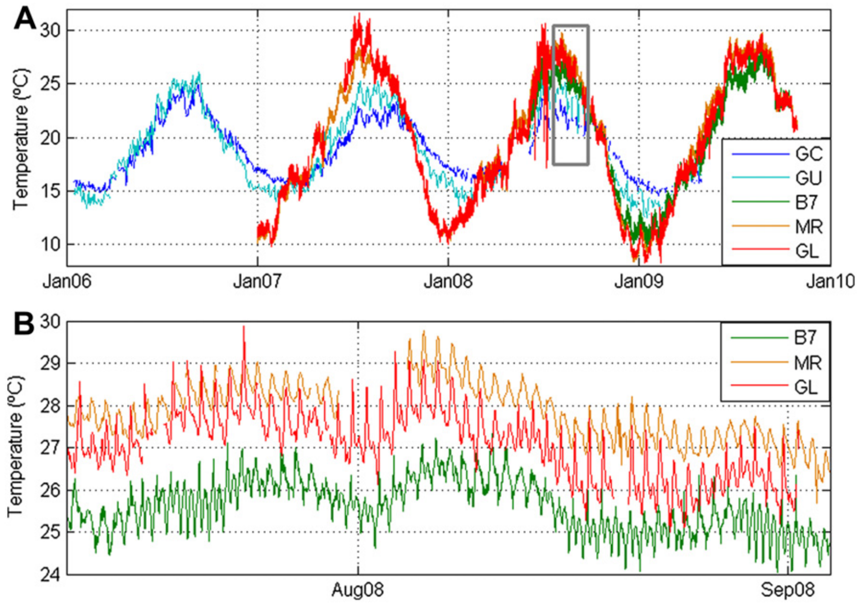


**Fig. 3.** (A) Temperature time series at the different locations considered in this work. Acronyms in the legend are the same as acronyms explained in Fig. 2. Temperature at GC and GU are spatial means of the daily SST provided by satellite observations. (B) Zoom of the observations inside the rectangle of panel A to show the tidal oscillations of temperature. Only sites B7, MR and GL, where sampling rate is enough to capture tidal oscillations, are shown in panel B.

## 3. Results and discussion

### 3.1. The temperature tidal signal

Fig. 4A shows the power spectral density of the local temperature at B7 after removing the seasonal contribution. The maximum value is achieved in the diurnal band although the amount of relevant lines in semidiurnal frequencies accounts for more explained variance in this band than in the diurnal one. Overall, 90% of the total variance in the range of tidal frequencies resides in these two bands, the rest being located in the bands of the non-linear constituents (species 3, 4, 5 etc.).

The length of the B7 time series allows for a good frequency resolution in the power spectrum and for the identification of single tidal constituents, which are indicated in Fig. 4. All them have been labeled according to their conventional name in the equilibrium tide. The relevant fact is that S1 is by far the most important line in the temperature spectrum (Fig. 4A). However, S1 is negligible in the tide generating potential. Actually the gravitational coefficient of S1 in the harmonic development of the equilibrium tide is 90 times smaller than O1 coefficient (Doodson, 1921; Cartwright and Tayler, 1971) while in Fig. 4A it is more than 30 times greater. This S1 signal is not gravitational, but radiational. The concept of radiational potential was introduced by Munk and Cartwright (1966) to account for tidal motions which are caused directly or indirectly by the sun's radiation. The strongest lines of the radiational potential are located at annual and diurnal frequencies, their effect being readily identifiable in Fig. 3. On the

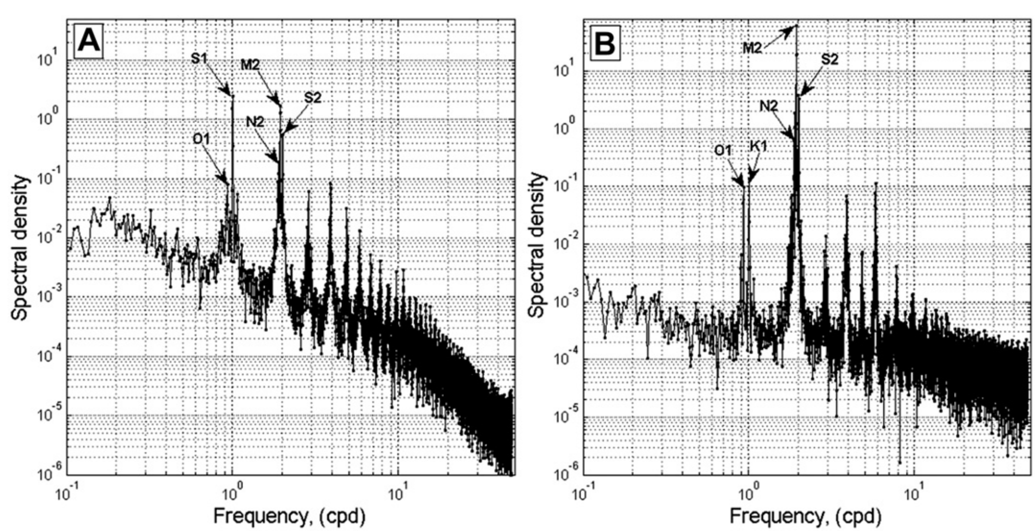


**Fig. 4.** (A) Power spectrum of the temperature series at B7 ($^{\circ}C^2$/cpd). Peaks of well defined frequency have been labeled according to their conventional names in tidal theory. (B) Same as (A) for the along-channel velocity of the uppermost level ($m^2\ s^{-2}$/cpd). Notice the different shape and relative importance of the lines in both spectra, panel (B) being more representative of the gravitational tide.

contrary, the lines lying in the semidiurnal band in Fig. 4, Fig. 3A, namely M2, S2 and N2, show relative amplitudes that agree with the values of the equilibrium tide, supporting – at least partially – their gravitational origin.

### 3.2. Source of the periodic signals

In a vertically well-mixed estuary the equation for local variations of temperature, which is deduced from the heat equation, can be written in one-dimensional form

$$\frac{\partial T}{\partial t}+u\frac{\partial T}{\partial x}=\frac{\partial}{\partial x}\left(\kappa_T\frac{\partial T}{\partial x}\right)+\frac{Q_T}{\rho c_p} \quad (1)$$

where $u$ is the instantaneous velocity, $\kappa_T$ is the turbulent diffusion coefficient of heat, $\rho$ is the water density, $c_p$ is the heat capacity of water and $Q_T$ is the heat power per volume unit (W m$^{-3}$) put into the water by external sources (short and long wave radiations, evaporation, etc.).

The terms in Eq. (1) able to generate the periodic signals observed in the power spectrum of Fig. 4A are the advective, $u\partial T/\partial x$, and the external source, $Q_T$, terms. The horizontal diffusion is negligible compared with the advective term. Actually, it is vertical diffusion that is important in the estuarine circulation, and this contribution has been implicitly taken into account in the well-mixed estuary hypothesis. Moreover and in case this term were not negligible, it is quite unlikely that it could introduce periodic signals. Regarding tidal and seasonal periodicity the origin of the periodic signals is the above mentioned terms and, therefore, the temperature equation for these frequencies reduces to

$$\frac{\partial T}{\partial t}=-u\frac{\partial T}{\partial x}+\frac{Q_T}{\rho c_p} \quad (2)$$

The nature of the periodic signals generated by the advective term is gravitational via the tidal currents forced by the vertical tide at the estuary mouth. The barotropic tide in the Gulf of Cadiz is clearly semidiurnal with an aspect ratio (O1 + K1)/(M2 + S2) less than 0.1, a result that is clearly echoed by the associated tidal currents, as it is shown by the relative importance of semidiurnal and diurnal lines in the power spectrum of Fig. 4B. Even when diurnal currents are still present in $u$, the smallness of the aspect ratio suggests that their contribution to temperature signal is negligible. Therefore the advective term (via the advective M2 dominance) is the main source of the semidiurnal signal, whereas term $Q_T/\rho c_p$ is responsible for the diurnal and, trivially, seasonal signals, whose origin is radiational. This last term, however, modifies the amplitude and phase of semidiurnal temperature signals through the temperature gradient $\partial T/\partial x$, which changes sign along the year as can be easily deduced from Fig. 3.

### 3.3. Temporal variability of the tidal signals

The main contributor to the external source term $Q_T/\rho c_p$ is the sun radiation, which has the seasonal cycle of the sun declination and also modulates the amount of daily incoming energy, i.e., the diurnal cycle. These facts along with the mentioned dependence of the temperature gradient on the sun radiation make the strength of the tidal signal change along the year. To investigate these changes, the original time series has been fitted to the harmonic model

$$T(t)=T_0+bt+\sum_i A_i\cos(\omega_i t-\varphi_i) \quad (3)$$

The summation includes harmonics with the frequencies of semidiurnal M2, S2, N2 and diurnal S1 constituents of the equilibrium tide ($i = 4$), which are the prevailing lines in Fig. 4A. Time origin is 1 of January 2008 at 00:00. The fitting was done for pieces one-month long, two consecutive pieces overlapped 15 days and the parameters of each single fitting were assigned to the central time of the piece. For one-month series, the seasonal cycle behaves like a short-term trend that is accounted for by term $bt$. Note that phases provided by Eq. (3) for the involved harmonics will not coincide with the phases deduced from classical tidal analysis packages such as T_Tide (Pawlowicz et al., 2002) for constituents M2, S2, N2 and S1. Phases in Eq. (3) are referred to the time origin of January 1st, 2008 while the classical analysis refers phases to the time when the associated fictitious stars transit over the Greenwich meridian.

Fig. 5 shows several remarkable features found in the temperature series of site B7. First, S1 has the greatest amplitude of all constituents during most of the period except for winter months (November 2008–February 2009, Fig. 5A) when it diminishes to values around 0.1 °C. It is M2 that dominates during this period with a peak value of 0.5 °C in January. Actually, S1 amplitude shows a seasonal cycle with larger amplitude in late spring and summer months.

Second, the phase of M2 changes abruptly by about 180° in late October 2008, then maintains a rather constant value until April 2009 when, again, changes quickly to the same values it showed before October 2008 (Fig. 5B). It is during this period that M2 reaches the absolute maximum. It is worth noting that both phase shifts take place when M2 amplitude shows close-to-zero minima (Fig. 5A). On the contrary, the phase of S1 remains nearly constant in spite of the marked seasonality of its amplitude.

Third, although supposedly the three semidiurnal constituents have gravitational origin, S2 behaves somewhat differently: during the short periods of M2 minima, S2 exceeds M2 amplitude, which has no explanation if the origin of both constituents were purely gravitational (M2/S2 amplitude ratio is 2.2 in the equilibrium tide). Also the 180° phase jump of M2 in spring and autumn is not mirrored by S2, which shows a much reduced phase shift of 80–90° on average. These facts suggest a radiational contribution to S2 signal that breaks the purely gravitational relationship between

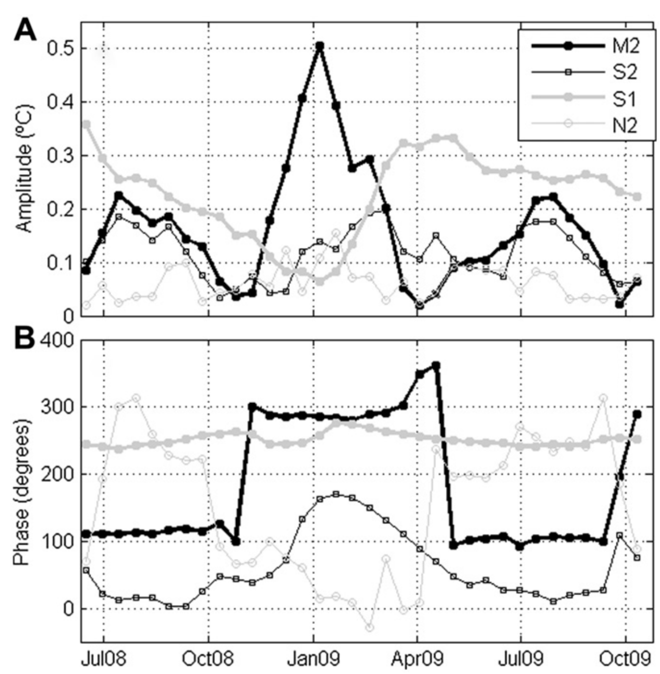


**Fig. 5.** (A) Amplitude as a function of time of the four harmonics included in the summation of Eq. (3) model at B7 (see legend) computed according to the procedure explained in the text. (B) Phase of these harmonics.

M2 and S2. Note that N2 behaves like M2 except for its much less amplitude. For this reason, N2 is not discussed any longer.

### 3.4. Time-variability of the harmonic constants

#### 3.4.1. The M2 case

The temperature tidal signal of M2 comes from the advective term $u\partial T/\partial x$. Its amplitude depends on the size of the M2 tidal current $u$, which is rather constant with time (last column of Table 1), and on the size of the temperature gradient $\partial T/\partial x$, which changes following a seasonal pattern (Fig. 6). The change of sign around April and October is the most noticeable property of this gradient, which gives place to the 180° shift of M2 phase in the temperature records. As a result of this change of sign, the amplitude of M2 is negligible or very small in short datasets of temperature collected in spring or autumn (see Table 1) when the temperature gradient is nearly null. It in turn implies that M2 amplitude has a semiannual modulation with two local maxima in winter and summer (Fig. 5A).

A striking consequence of this modulation is the almost null amplitude of M2 obtained when analyzing long time series of temperature, either using the model of Eq. (3) or classical tidal harmonic analysis techniques. Last row of Table 1 illustrates this result when applying the T_Tide software to the B7 temperature series. In this case, the presence of H1 and H2 constituents in the tide generating potential gives rise to a second surprising result, which is summarized in the footnote of Table 1. H1 and H2 frequencies are $f_{H1} = 1.9295$ cycles per day (cpd) and $f_{H2} = 1.9350$ cpd, one cycle per year smaller and greater than M2 frequency, $f_{M2}$, respectively. In the classical harmonic analysis these constituents are resolved from M2 in one-year or longer time series, but their coefficients in the equilibrium tide relative to M2 are so low ($C_{H1}/C_{M2} = 0.0035$; $C_{H2}/C_{M2} = 0.0030$, see Cartwright and Tayler (1971)) that they are always ignored. Here things are a bit different: since H1 and H2 have nearly the same frequency and amplitude, their superposition originates a signal of frequency $[f_{H1} + f_{H2}]/2$, which is just $f_{M2}$, that beats with a period of $[f_{H2} - f_{H1}]^{-1}$ or half a year, which is the temporal pattern exhibited by M2 temperature signal at B7. For this reason and in order to explain the beating nature of M2, the classical harmonic analysis ascribes M2 energy to its neighbor constituents H1 and H2, which now show amplitudes three times greater than M2 (footnote of Table 1). Note that this is a necessary mathematical artifact of the least-square fitting to explain the 180° phase shift shown in Fig. 5B, although the actual energy resides exactly at M2 frequency.

#### 3.4.2. The S1 case

Fig. 7 shows a seasonal pattern with larger amplitudes of S1 in late spring–summer, a fact that stems from the greater number of daylight hours in these months. Fig. 7A shows a contradictory result regarding the spatial dependence of S1 amplitude. On one hand, it suggests that the more upstream we move, the greater the amplitude, although it could also happen that the much larger amplitude observed in MR were a local effect (MR is located in the confluence of a secondary channel with the main channel of the estuary, see Fig. 2). On the other hand the amplitudes at B7 (near the estuary mouth) and GL (well upstream) are very similar, which suggests no or very weak spatial dependence. More information along the river is necessary to elucidate this contradiction. The phase of S1 (Fig. 7B) is rather stable with values around 300° and a steady increase from the mouth upstream, indicating that the local daily maximum takes place a bit earlier in the estuary mouth than upstream.

The larger daily oscillation in summer is the result of the enhanced heat gain by the absorption of solar radiation in this season. The oscillation does not follow a regular sinusoidal shape but a quick increase during the light hours followed by an also sharp decrease during night. Though periodic, this kind of signal is rich in high-order harmonics, a fact clearly visible in the power spectrum of Fig. 4A. It is of particular concern for the first harmonic of S1 (let us call it $S2_R$) because it has exactly the same frequency as the gravitational contribution S2, which is the next important constituent in the gravitational potential after M2.

#### 3.4.3. The S2 case

This harmonic has both gravitational and radiational contributions (first and second terms of the rhs of Eq. (2), respectively). A separation of both contributions has been made according to the following procedure. The time derivative of temperature at B7 has been computed (lhs of Eq. (2)), the resulting time series has been divided into pieces and analyzed to estimate a time series of amplitude and phase of M2 and S2 harmonics, as explained in Section 3.3. Let us call these series $(\partial T/\partial t)_{M2}$ and $(\partial T/\partial t)_{S2}$, respectively. The velocity amplitude and phase of M2 and S2 harmonics, $u_{M2}$ and $u_{S2}$, have been estimated from the ADP velocity record following the same procedure. Note that the these harmonics have gravitational origin exclusively.

Since $(\partial T/\partial t)_{M2}$ is gravitational, then it verifies that $(\partial T/\partial t)_{M2} = (u\partial T/\partial x)_{M2}$ and the temperature gradient $\partial T/\partial x$ can be readily computed as

$$\frac{\partial T}{\partial x} = \frac{\left(\partial T/\partial t\right)_{M2}}{u_{M2}} \tag{4}$$

(note that an equation similar to Eq. (4) for S2 cannot be applied). Using this value of $\partial T/\partial x$, the gravitational contribution of S2 is then estimated as

**Table 1**
Harmonic constants of temperature for S1, M2 and S2 constituents and velocity at 1 m depth for M2 constituent (last column) recorded at site B7, deduced from the classical harmonic analysis (T_Tide, Pawlowicz et al., 2002) applied to pieces of approximately two-month length spanning different periods of the year (first column). The 95% confidence interval of the estimated constant is shown between brackets. Blank cells indicate no-significant values of the harmonic constants. Last row, in bold, shows the harmonic constants of the whole 17-month time series.

| Time span | S1 ($T$) | | M2 ($T$) | | S2 ($T$) | | M2 ($u$) | |
|---|---|---|---|---|---|---|---|---|
| | Amp (°C × 100) | Phase (deg.) | Amp (°C × 100) | Phase (deg.) | Amp (°C × 100) | Phase (deg.) | Amp (cm s$^{-1}$) | Phase (deg.) |
| 1.Jul.08–28.Aug.08 | 38.4 (2.8) | 266 (6) | 20.2 (1.7) | 315 (5) | 17.0 (1.7) | 16 (6) | 100.7 (4.1) | 49 (3) |
| 25.Sep.08–17.Nov.08 | 22.2 (1.8) | 275 (12) | – | – | 4.1 (2.6) | 36 (36) | 98.1 (6.1) | 50 (4) |
| 13.Dec.08–14.Feb.09 | 12.1 (2.5) | 282 (18) | 39.0 (3.8) | 130 (6) | 13.3 (3.8) | 160 (17) | 102.9 (4.2) | 46 (3) |
| 14.Mar.09–16.May.09 | 50.0 (2.4) | 279 (4) | 4.8 (3.1) | 294 (38) | 9.7 (3.2) | 75 (19) | 112.8 (5.9) | 52 (3) |
| 30.Jun.09–31.Aug.09 | 38.6 (3.4) | 267 (6) | 20.1 (3.5) | 309 (10) | 16.2 (3.5) | 20 (12) | 92.7 (3.5) | 47 (3) |
| **1.Jun.08–24.Oct.09** | **32.5 (1.0)** | **276 (3)** | **4.7* (1.3)** | **131 (16)** | **6.4 (1.3)** | **76 (12)** | **103.5 (1.1)** | **49 (1)** |

* For time series longer than one year, M2 energy is transferred to the neighbor H1 and H2 constituents, which now have amplitudes of 13.5 ± 1.3 and 14.0 ± 1.3 (°C × 100), respectively, and phases of 299 ± 5 and 142 ± 5 (degrees), respectively. See text for more explanations.

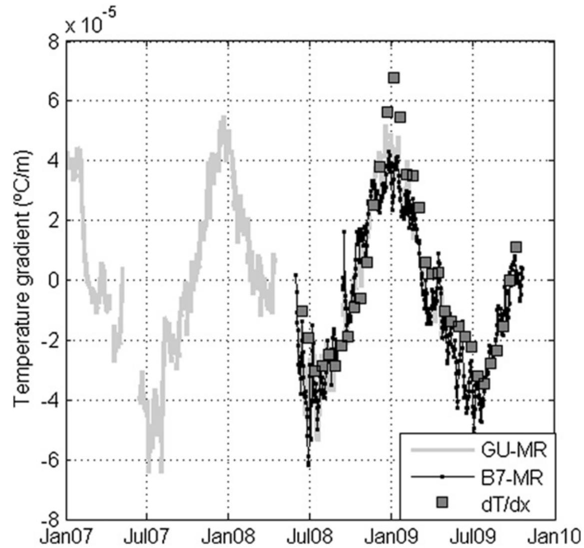


**Fig. 6.** Temperature difference per unit distance between the GU area in the open ocean and MR station upstream in the river (see Fig. 2 for location), between site B7 and MR station, and temperature gradient computed through Eq. (4). The legend identifies the different lines.

$$\left(\frac{\partial T}{\partial t}\right)_{S2,G} \equiv \left(u\frac{\partial T}{\partial x}\right)_{S2,G} = u_{S2}\frac{\partial T}{\partial x} \tag{5}$$

and the radiational part as

$$\left(\frac{\partial T}{\partial t}\right)_{S2,R} \equiv \left(\frac{Q_T}{\rho c_p}\right)_{S2,R} = \left(\frac{\partial T}{\partial t}\right)_{S2} - \left(\frac{\partial T}{\partial t}\right)_{S2,G} \tag{6}$$

Fig. 8A and B present the amplitude and phase of each term. The radiational contribution exceeds the gravitational one except for a short period in winter and shows an annual cycle like S1, while the gravitational counterpart has a rather clear semiannual pattern like M2. On average and according to this decomposition, the radiational contribution prevails in the S2 signal of temperature (65% *versus* 35% of the gravitational part).

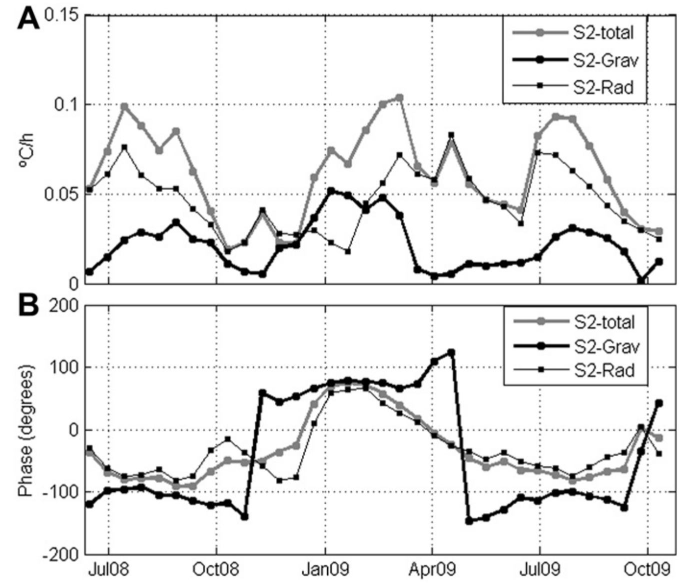


**Fig. 8.** Decomposition of S2 tidal signal in their gravitational and radiational contributions at B7. (A) Amplitude. (B) Phase. Amplitude units are °C per unit time (hour) since the analysis has been performed on the time derivative of temperature. Accordingly, phase values are 90° out of phase with respect to Fig. 5.

### 3.5. The horizontal temperature gradient

Fig. 6 shows the temperature difference per unit distance between GU and station MR and between sites B7 and MR. Both curves change sign seasonally. Those differences will coincide with the horizontal temperature gradient if it is uniform, otherwise they will not, although they will still be a good proxy of the gradient. The -local- temperature gradient deduced from Eq. (4) is also plotted and presents an encouraging similitude with the temperature differences. It is important because the feasibility of the procedure followed to compute the gradient depends on the validity of Eq. (1) and on the fact that all M2 variability resides in the advective term $u\partial T/\partial x$. The good agreement between the temperature differences

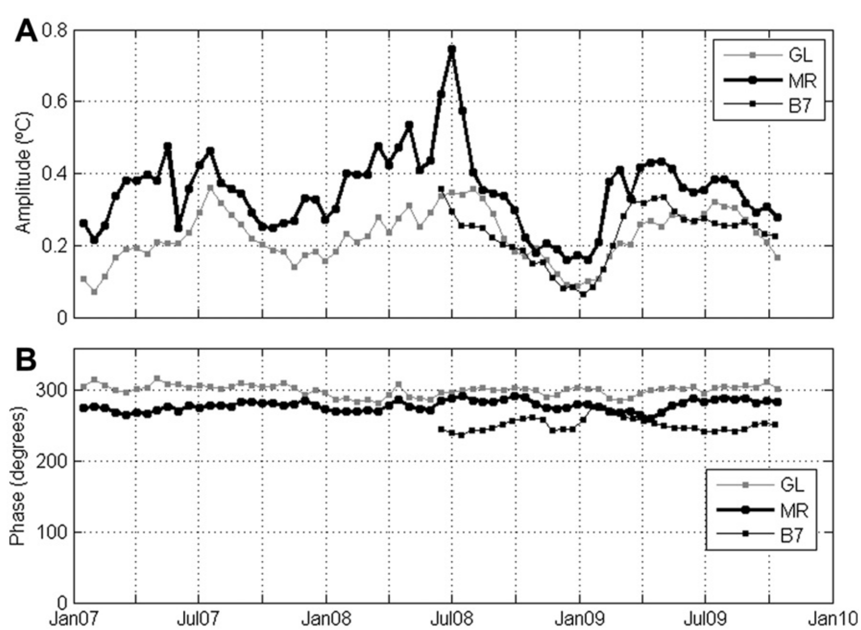


**Fig. 7.** Amplitude (panel A) and phase (B) of harmonic S1 at stations B7, MR and GL, as a function of time.

and the local gradient strongly suggests that both conditions are fulfilled satisfactorily.

The temperature difference per unit distance and the local gradient shown in Fig. 6 are strikingly similar during most of the year but they differ in winter months when the local gradient may be 50% higher. It suggests that the temperature gradient is uniform and equal to the local gradient at B7 during most of the year, and the estuary temperature would change linearly from the mouth to MR station, more than 60 km upstream. The situation changes in winter when, judging from the temperature gradient at B7, the greatest part of the temperature difference would be achieved nearby the estuary mouth, the rest of the estuary remaining fairly homogeneous and noticeably cooler than the ocean in this season.

## 4. Conclusions

In the vicinity of the mouth of a tidally-driven estuary in mid-latitudes, the direct and indirect influence of sun's radiation makes the amplitude and phase of the prevailing tidal constituents of local temperature records computed by standard harmonic analysis be fairly dependent on the length and epoch of the year of the collected data. Table 1 shows this dependence in the case of Guadalquivir river, southwest Spain, by presenting the harmonic constants computed for several pieces extracted from the temperature time series at site B7 (near the estuary's mouth) that have been processed following the broadly used classical analysis described in Foreman (1977) or Pawlowicz et al. (2002).

Semidiurnal constituents come from the advective term, which is the product of the tidal velocity times the horizontal temperature gradient. This gradient changes sign seasonally and passes through zero twice a year, which implies very small amplitude of the local temperature signal in semidiurnal constituents if we analyze a time series of short length centered around the dates when the gradient cancels (April and October, see Fig. 6; see also second and fourth rows in Table 1). Another curious result is the very small amplitude of M2 that is obtained when analyzing series one year long or greater. The energy residing in M2 frequency is diverted to the neighbor constituents H1 and H2 that differ from M2 by 1 cycle per year.

The most important constituent, however, is S1, of radiational origin, which shows a seasonal cycle with larger amplitudes in summer, a result directly related to the greater amount of daylight hours in this season. The S1 oscillation is far from being sinusoidal and therefore it is rich in high order harmonics (Fig. 4). This asymmetry affects S2 constituent, which usually has a prevailing gravitational contribution (equilibrium tide). In this case, the larger contribution comes from the radiational potential via the first harmonic of S1 ($S2_G$), which shows to be nearly twice the gravitational counterpart.

Finally and considering the relevant role of $(\partial T/\partial x)$ in the tidal signal of temperature, we have carried out a satisfactory and encouraging comparison between a spatially averaged gradient, computed as the difference of temperature between a station well upstream and our station near the estuary's mouth divided by the distance, and the indirect and independent estimation of the local temperature gradient by means of Eq. (4). The local gradient in winter is, however, significantly greater than the spatially averaged gradient, which indicates a non-homogeneous gradient enhanced near the mouth of the estuary. The result deserves an additional comment. Contrary to what happens with salinity, temperature advection can be downstream (summer) or upstream (winter). Salinity is always transported upstream (the salt source is the ocean) and the mechanism is the well-known tidal pumping or the positive correlations between tidal oscillations of salinity and tidal currents. In winter months, when the ocean is also the source of heat, salinity and temperature must behave similarly and the same mechanism must operate for the upstream transport of heat (i.e., temperature). The enhanced gradient of temperature near the mouth is, therefore, an indirect evidence of the fast decay of the salinity intrusion, which would be restricted to the last few kilometers of the estuary.

## Acknowledgments

Partial financial funding from the Spanish Ministry of Science and Innovation through CTM2010-21229-C02-01, CTM2008-04150/E projects and also from Regional Andalucía Government P08-RNM-03738 project are acknowledged. This is the publication no. 10 from CEIMAR Publication Series.

## References

Alvarez, O., Tejedor, B., Vidal, J., 2001. La dinámica de marea en el estuario del Guadalquivir: un caso peculiar de "resonancia antrópica. Física de la Tierra 13, 11–24 (in Spanish).

Cartwright, D.E., Tayler, R.J., 1971. New computations of the tide generating potential. Geophysical Journal of the Royal Astronomical Society 23, 45–74.

Davies, J.L., 1964. A morphogenic approach to the worlds' shorelines. Zeitschrift für Geomorphologie 8, 127–142.

Doodson, A.T., 1921. The harmonic development of the tide-generating potential. Proceedings of the Royal Society A 100, 305–329.

Foreman, M.G.G., 1977. Manual for Tidal Heights Analysis and Prediction. Pacific Marine Science Report 77–10. Institute of Ocean Sciences, Patricia Bay, Sidney B.C., 58 pp.

García-Lafuente, J., Almazan, J.L., Fernandez-Castillejo, F., Kribeche, A., Hakimi, A., 1990. Sea level in the Strait of Gibraltar: tides. International Hydrographic Review LXVII (1), 111–130.

García-Lafuente, J., Del Río, J., Alvarez Fanjul, E., Gomis, D., Delgado, J., 2004. Some aspects of the seasonal sea level variations around Spain. Journal of Geophysical Research 109, C09008. http://dx.doi.org/10.1029/2003JC002070.

García-Lafuente, J., Ruiz, J., 2007. The Gulf of Cádiz pelagic ecosystem: a review. Progress in Oceanography 74, 228–251. http://dx.doi.org/10.1016/j.pocean.2007.04.001.

Munk, W.H., Cartwright, D.E., 1966. Tidal espectroscopy and prediction. Philosophical Transactions of the Royal Society A 259, 533–581.

Navarro, G., Gutiérrez, F.J., Díez-Minguito, M., Losada, M.A., Ruiz, J., 2011. Temporal and spatial variability in the Guadalquivir estuary: a challenge for a real-time telemetry. Ocean Dynamics 61 (6), 753–765. http://dx.doi.org/10.1007/s10236-011-0379-6.

Navarro, G., Huertas, I.E., Costas, E., Flecha, S., Díez-Minguito, M., Caballero, I., López-Rodas, V., Prieto, L., Ruiz, J., 2012. Use of a real-time remote monitoring network (RTRM) to characterize the Guadalquivir estuary (Spain). Sensors 12 (2), 1398–1421.

Pawlowicz, R., Beardsley, B., Lentz, S., 2002. Classical tidal harmonic analysis including error estimates in MATLAB using T_Tide. Computers and Geosciences 28 (8), 929–937.

Rodríguez-Ramirez, A., Yáñez-Camacho, C.M., 2008. Formation of chenier plain of the Doñana marshland (SW Spain): observations and geomorphic model. Marine Geology 254, 187–196. http://dx.doi.org/10.1016/jmargeo.2008.06.006.

Ruiz, J., García-Isarch, E., Huertas, E.I., Prieto, L., Juárez, A., Muñoz, J.L., Sánchez-Lamadrid, A., Rodríguez-Gálvez, S., María-Naranjo, J., Baldó, F., 2006. Meteorological and oceanographic factors influencing *Engraulis encrasicolus* early life stages and catches in the Gulf of Cádiz. Deep Sea Research Part II 53 (11–13), 1363–1376.

Vargas, J.M., García-Lafuente, J., Delgado, J., Criado, F., 2003. Seasonal and wind-induced variability of sea surface temperature patterns in the Gulf of Cádiz. Journal of Marine Systems 38, 205–219.